The Astrophysical Journal Supplement Series, 216:3 (8pp), 2015 January doi:10.1088/0067-0049/216/1/3
© 2015. The American Astronomical Society. All rights reserved.

LABORATORY STUDY OF RATE COEFFICIENTS FOR H_2O:He INELASTIC COLLISIONS BETWEEN 20 AND 120 K

G. Tejeda[1], E. Carmona-Novillo[2], E. Moreno[1], J. M. Fernández[1], M. I. Hernández[2], and S. Montero[1]
[1] Laboratory of Molecular Fluid Dynamics, Instituto de Estructura de la Materia, CSIC Serrano 121, E-28006 Madrid, Spain
[2] Instituto de Física Fundamental, CSIC Serrano 123, E-28006 Madrid, Spain; emsalvador@iem.cfmac.csic.es
Received 2014 August 2; accepted 2014 November 3; published 2014 December 16

ABSTRACT

State-to-state rate coefficients for ortho-H_2O:He and para-H_2O:He inelastic collisions in the 20–120 K thermal range are investigated by means of an improved experimental procedure. This procedure is based on the use of a kinetic master equation (MEQ) which describes the evolution of populations of H_2O rotational levels along a supersonic jet of H_2O highly diluted in helium. The MEQ is expressed in terms of experimental observables and rate coefficients for H_2O:He inelastic collisions. The primary experimental observables are the local number density and the populations of the rotational energy levels of H_2O, quantities which are determined along the jet with unprecedented accuracy by means of Raman spectroscopy with high space resolution. Sets of rate coefficients from the literature and from present close-coupling calculations using two different potential energy surfaces (PESs) have been tested against the experiment. The Green et al. rate coefficients are up to 50% too low compared to the experiment, while most rates calculated here from the Hodges et al. PES and the Patkowski et al. PES are much closer to the experimental values. Experimental rates with an estimated accuracy on the order of 10% have been obtained for ortho-H_2O:He and para-H_2O:He inelastic collisions between 20 and 120 K by scaling and averaging the theoretical rates to the experiment.

Key words: astronomical databases: miscellaneous – ISM: molecules – methods: laboratory: molecular – molecular processes – techniques: spectroscopic

Supporting material: machine-readable tables

1. INTRODUCTION

Water, the third most abundant molecule in the interstellar medium, is a fundamental observational target in present-day astrophysics and astrochemistry (WISH 2010; Roueff & Lique, 2013). The collisional excitation of water by light projectiles like H, H_2, or He, is a fundamental energy transfer mechanism where ortho-H_2O:He and para-H_2O:He state-to-state rate coefficients (STS rates, in short) are relevant for modeling the physical conditions of water-rich regions. Hitherto, this task has been supported by STS rates calculated from theoretical methods (Green et al. 1993; Yang et al. 2013). However, since these STS rates strongly depend on the quality of the H_2O–He intermolecular potential energy surface (PES) employed in the calculation, substantial differences can be expected for the STS rates derived from the various H_2O–He PESs published so far (Palma et al. 1988; Maluendes et al. 1992; Hodges et al. 2002; Patkowski et al. 2002; Calderoni et al. 2003; Makarewicz 2008; Roncaratti et al. 2009), even employing the essentially accurate close-coupling methodology. Moreover, the accuracy of such results is conjectural since no systematic comparison to experiments has been possible so far. A preliminary indirect validation of Green et al. (1993) STS rates based on spectral line broadening data of ortho- and para-H_2O transitions in the 0.55 to 1.17 THz domain and the thermal range between 60 and 220 K has been reported (Dick et al. 2009, 2010). On the other hand, several H_2O:He differential cross sections suitable for comparison with theoretical results have been obtained from crossed beam experiments of H_2O with He (Brudermann et al. 2002; Yang et al. 2010a, 2010b). No other experimental data related to H_2O:He inelastic collisions are known to the authors.

The first goal of the present work is to show the scope of an improved experimental validation procedure for theoretical H_2O:He STS rates. The second goal is to provide experimental STS rates for ortho- and para-H_2O:He inelastic collisions in the vibrational ground state of H_2O for the 20–120 K thermal range. Three sets of STS rates are tested in the present work, namely, that by Green et al. (1993) and those calculated in the present work within the close-coupling approach by employing the MOLSCAT code (Hutson & Green, 1994), with the H-PES (SIII surface) of Hodges et al. (2002) and the P-PES of Patkowski et al. (2002). These three sets of theoretical STS rates will be henceforth referred to as *G*-rates, *H*-rates, and *P*-rates.

2. METHODOLOGY

The present experimental methodology relies on the kinetic master equation (MEQ)

$$\frac{dP_i}{dt} = n \sum_{\ell} (-P_i k_{i\to\ell} + P_\ell k_{\ell\to i}), \quad (1)$$

which describes the time evolution of the population P_i of the ith rotational quantum level of either ortho- or para-H_2O as a consequence of inelastic collisions in the gas of water molecules infinitely diluted in a bath of helium atoms at an instantaneous number density n and translational temperature T_t. In the supersonic jet experiments described below, this T_t is defined via the distribution function of molecular velocities referred to the local flow velocity, i.e., fully equivalent to the translational temperature in a static gas sample. The ks in Equation (1) are the T_t-dependent STS rates accounting for the elementary collision process

$$H_2O(i) + He \xrightarrow{k_{i\to\ell}} H_2O(\ell) + He, \quad (2)$$

Table 1
Identification of Rotational Energy Levels of $H_2{}^{16}O$ in the Vibrational Ground State

ortho-H_2O						para-H_2O					
i	E_i (cm^{-1})	J	τ	K_a	K_c	i	E_i (cm^{-1})	J	τ	K_a	K_c
1	23.7944	1	−1	0	1	1	0.0000	0	0	0	0
2	42.3717	1	1	1	0	2	37.1371	1	0	1	1
3	79.4964	2	−1	1	2	3	70.0908	2	−2	0	2
4	134.9016	2	1	2	1	4	95.1759	2	0	1	1
5	136.7617	3	−3	0	3	5	136.1639	2	2	2	0
6	173.3658	3	−1	1	2	6	142.2785	3	−2	1	3
7	212.1564	3	1	2	1	7	206.3014	3	0	2	2
8	224.8384	4	−3	1	4	8	222.0527	4	−4	0	4
9	285.4186	3	3	3	0	9	275.4970	4	−2	1	3
10	300.3623	4	−1	2	3	10	285.2193	3	2	3	1
11	325.3479	5	−5	0	5	11	315.7795	4	0	2	2
12	382.5169	4	1	3	2	12	326.6255	5	−4	1	5
13	399.4575	5	−3	1	4	13	383.8425	4	2	3	1

Note. After Tennyson et al. (2001).

between a molecule of either ortho- or para-H_2O in the precollisional quantum state i and a helium atom, undergoing the H_2O molecule transition to the postcollisional quantum state ℓ with a variation of the kinetic energy of the partners as a consequence of the collision.

The STS rates in Equation (1) obey the detailed balance relation

$$k_{i\to\ell} = k_{\ell\to i}\frac{(2J_\ell+1)}{(2J_i+1)}\times e^{-(E_\ell-E_i)/k_BT_t}, \quad (3)$$

where J_i and J_ℓ are the rotational angular momentum quantum numbers of either ortho- or para-H_2O, and E_i and E_ℓ are the energies of the rotational levels. For $E_\ell > E_i$, $k_{\ell\to i}$ and $k_{i\to\ell}$ account for de-excitation and excitation elementary processes, respectively. The identification of the energy levels of $H_2{}^{16}O$ considered in the present work is given in Table 1.

Equation (1) obeys a fundamental matter conservation principle and holds to a very good approximation if the number of triple collisions is negligible, and the evolution of populations is so fast that radiative processes are irrelevant. Both conditions are satisfied in the experiments described below.

In the present work, Equations (1) and (3) apply to the paraxial region of a supersonic free jet of helium seeded with 1.4% of natural (3:1 ortho to para ratio) water vapor. The rotational populations P_i are normalized here as $\sum_i P_i = 3/4$ for ortho-H_2O and $\sum_i P_i = 1/4$ for para-H_2O.

In order to investigate the STS rates of the MEQ (1) at a translational temperature T_t, Equations (1) and (3) apply to the particular paraxial point z of the jet where the local temperature is T_t. At this very same point z, the left-hand term dP_i/dt's (LHT_i's), and the number density n and the P_i rotational populations in the right-hand term (RHT_i's) of MEQ (1) can be obtained locally via experiment with unprecedented accuracy by means of Raman spectroscopy with high space resolution (Fonfría et al. 2007; Pérez-Ríos et al. 2011; Tejeda et al. 2012). The only unknowns are then the STS rates in the RHT of the MEQ (1).

We proceed as follows. First, any set of preexisting STS rates for H_2O:He inelastic collisions at a temperature T_t, e.g., the G-rates, H-rates, and P-rates considered here, can be assessed in a straightforward manner via experiment by means of Equations (1) and (3). As a measure of the quality of any of these sets, we employ the sum of a squared residual's differences

$$\chi^2(T_t) = \sum_{i=1}^{m}(\mathrm{LHT}_i - \mathrm{RHT}_i)^2, \quad (4)$$

where every LHT_i is a purely experimental quantity (dP_i/dt), while the corresponding RHT_i is a combination of experimental quantities (n and P_i) and STS rates. Index i in Equation (4) runs over the subset of the m lowest rotational levels of either ortho-H_2O or para-H_2O. In this work, the subset of levels tested corresponds to i = 1–8 of both H_2O species, where most of the rotational population is concentrated and the signal-to-noise ratio of the Raman spectra is good enough. The smaller the parameter $\chi^2(T_t)$, the better is the tested sets of STS rates at temperature T_t. Via this procedure, we immediately establish that for $20 \leqslant T_t \leqslant 120$ K, the P-rates and the H-rates are far better than the G-rates.

In order to determine a set of experimental STS rates, we take advantage of the strong correlation between pairs of STS rates from close-coupling calculations based on different PESs. As a sample case, the pair correlations of P-rates with G-rates, H-rates with G-rates, and P-rates with H-rates for ortho-H_2O:He collisions at $T_t = 120$ K are shown in Figure 1. Similar correlations are found at $20 \leqslant T_t \leqslant 120$ K for ortho- and para-H_2O:He collisions. For any particular temperature T_t, we conclude the following from these correlations.

1. The relative values of different STS rates calculated in the close-coupling approach depend largely on the pre- and post-collisional rotational quantum numbers of H_2O and are little sensitive to the PESs employed in the calculation. Hence, the relative values of the calculated STS rates are good approximations regardless of the PES. As shown in Figure 1, this is reflected by the high value of the determination coefficient $R_{sq} > 0.99$ of the linear regression.
2. The homologous STS rates calculated from different PESs in the frame of the close-coupling approach are, to a good approximation, proportional by a constant factor. The slope of the pair regression line largely depends on the anisotropies of both PESs and is nearly independent of the pre- and post-collisional rotational quantum numbers of H_2O and on the long-range behavior of the PESs. As shown in Figures 1(a)–(c), the P-PES is considerably more anisotropic than the G-PES, and the H-PES is more anisotropic than the G-PES but slightly less anisotropic than the P-PES.

On this basis, any preexisting set of calculated STS rates (here the G-rates, H-rates, and P-rates) at temperature T_t can be scaled to the experiment by a single factor F that minimizes χ^2 according to Equation (4). As shown in the example of Figure 2 for ortho-H_2O:He collisions at 120 K, χ^2 show well determined minima for the G-rates, H-rates, and P-rates assessed here. Note that in all three cases, the minima of χ^2 is unambiguously within the range $0.5 \leqslant F \leqslant 2$, implying that the G-rates, H-rates, and P-rates calculated from the G-PES, H-PES, and P-PES, respectively, are in the right order of magnitude. The experimental factors F_G, F_H, and F_P, which minimize χ^2 for the G-rates, H-rates and P-rates between 20 and 120 K, are given in Table 2.

An important result of this procedure is that the scaled rates, besides minimizing $\chi^2(T_t)$, are much closer among them than the original ones. The average of the three sets of STS rates

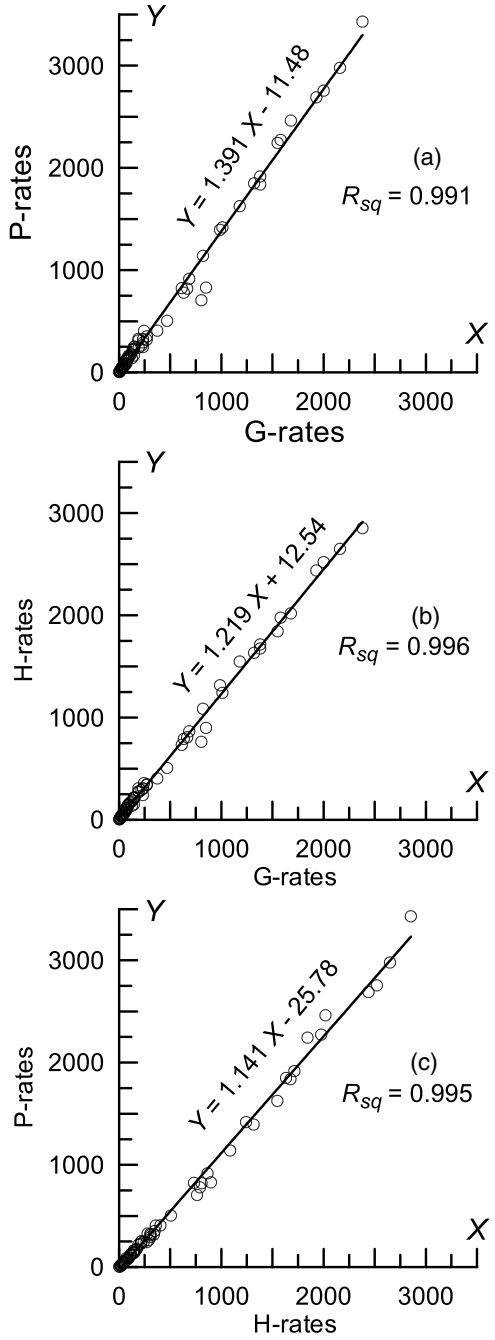

Figure 1. Pair correlation of *G*-rates, *H*-rates, and *P*-rates for ortho-H_2O:He deexcitation collisions at $T_t = 120$ K. All 68 $k_{\ell\to i}$ rates with $\ell > i$, $(2 \leqslant \ell \leqslant 13)$, $(1 \leqslant i \leqslant 8)$ are included. Rates are in units of 10^{-14} cm^3 s^{-1}.

Table 2
Experimental Scaling Factors F for the Theoretical *G*-rates, *H*-rates, and *P*-rates

	ortho-H_2O:He			para-H_2O:He		
T_t/K	F_G	F_H	F_P	F_G	F_H	F_P
20	1.62	1.17	0.98	1.66	1.32	1.11
40	1.41	1.08	0.92	1.36	0.91	0.85
60	1.50	1.17	1.05	1.26	1.02	1.00
80	1.41	1.11	1.00	1.12	0.92	0.90
100	1.47	1.17	1.08	1.13	0.93	0.91
120	1.53	1.22	1.14	1.26	1.02	1.0
Average	1.49 ±0.08	1.15 ±0.05	1.03 ±0.08	1.30 ±0.20	1.02 ±0.16	0.96 ±0.09

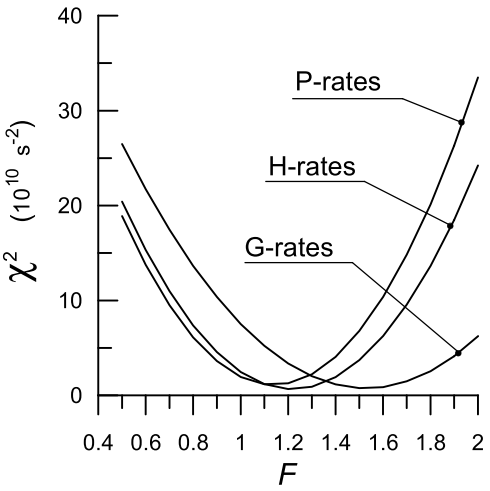

Figure 2. ortho-H_2O:He inelastic collisions at 120 K: χ^2 as a function of the scaling factor F for *G*-rates, *H*-rates, and *P*-rates.

scaled to the experiment (SE)

$$k^{SE}_{\ell\to i} = \left(F_G k^G_{\ell\to i} + F_H k^H_{\ell\to i} + F_P k^P_{\ell\to i}\right)/3, \quad (5)$$

can be considered as the best experimental approximation to the STS rates for the H_2O:He collisions in the $20 \leqslant T_t \leqslant 120$ K range. A measure of the probable uncertainty of the $k^{SE}_{\ell\to i}$ experimental STS rates is given by

$$\delta k^{SE}_{\ell\to i} = \left(\left[\left(k^{SE}_{\ell\to i} - F_G k^G_{\ell\to i}\right)^2 + \left(k^{SE}_{\ell\to i} - F_H k^H_{\ell\to i}\right)^2 + \left(k^{SE}_{\ell\to i} - F_P k^P_{\ell\to i}\right)^2\right]/2\right)^{1/2}. \quad (6)$$

3. EXPERIMENTAL DETAILS

Experimental work has been conducted in one of the two dedicated facilities for quantitative gas diagnostics which are operative at the Laboratory of Molecular Fluid Dynamics (IEM-CSIC, Madrid). A simplified scheme of the facility is shown in Figure 3, where numbers refer to parts described below.

The apparatus is based on an expansion chamber (1) evacuated by a high-capacity clean vacuum line (2, 2′, 2″). Steady supersonic-free jets are produced in the chamber by the expansion of the gas mixture through a $D = 350\,\mu$m xyz-movable nozzle (3) which is fed by an $He + H_2O$ supply line (4). The Raman scattering was excited at selected points along the jet with step-size $\Delta z = 100 \pm 1\,\mu$m by a 10 W ($\lambda = 532$ nm) single-mode *cw*-laser (5). The wavenumbers and intensities of the Raman scattering spectral lines were measured by a very high-sensitivity double-grating spectrometer (6) of 0.1 cm^{-1} resolution, which is equipped with a low-noise CCD detector refrigerated by liquid-N_2. The laser source, the expansion chamber, and the spectrometer are mechanically isolated from each other in order to avoid propagation of vibrations from the vacuum pumps, but are optically connected by a highly efficient optical transfer system (7, 7′, 7″). The nozzle was operated at $T \approx 360$ K and stabilized to ±0.1 K by means of a closed loop system (not shown in Figure 3). Reference pressures (≈10 mbar) in the expansion chamber were measured by an MKS Baratron (8) of ±0.01 mbar accuracy. The shape and size of the probed gas volume is shown in the inset of Figure 3(b).

The present experimental procedure conveys a number of substantial advantages compared to other methods aimed at studying inelastic collisions. Based on the combination of steady supersonic jets and state-of-the-art Raman spectroscopy with high

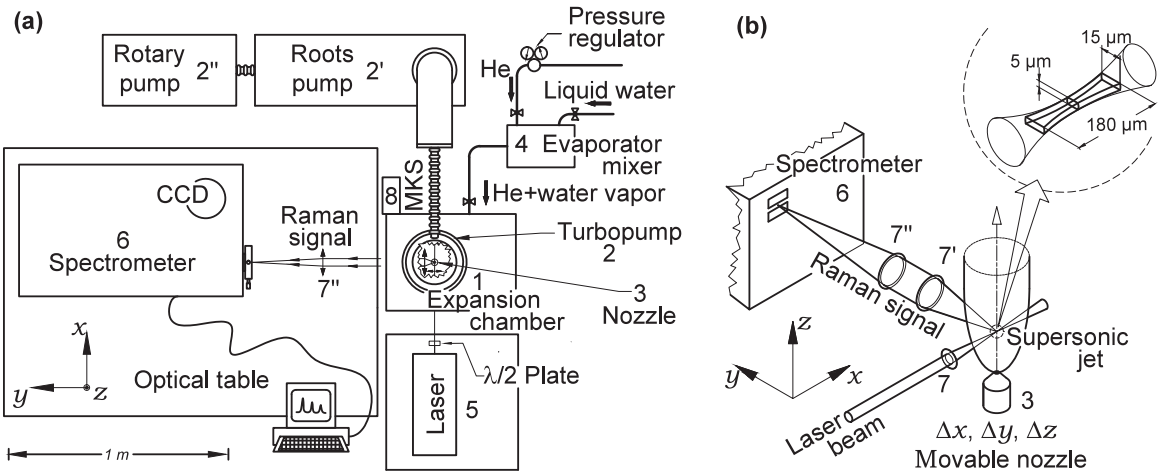

Figure 3. Experimental set up with (a) a general view and (b) a detail of the nozzle, supersonic jet, and probed gas volume.

spatial resolution, the tiny volume of gas probed where the effect of the collisions is studied (inset of Figure 3(b)) shares much in common with the interstellar medium. First, by virtue of the gas-dynamic properties of the paraxial region of the supersonic jet, the molecules are self-confined and free from interaction with cell walls or with other warmer or colder molecules traveling upstream or downstream of the probed gas volume. Second, the supersonic expansion provides a natural way of cooling the target molecules down to temperatures that are beyond the scope of static gas techniques; furthermore, temperatures are smoothly correlated with the distance z of the probed point to the nozzle. Third, since the paraxial zone of the jet is laminar, the local flow velocity can be accurately determined, and distance z along the jet provides a high-accuracy timescale in the domain of nanoseconds. Fourth, since the Raman scattering cross sections are very small, the perturbation of the probed gas volume is negligible. Thus, our experiment truly measures the local properties of the gas: number density, translational temperature, flow velocity, rotational populations, and their time dependence. These quantities were measured as follows.

Local number densities $n(z)$ were measured along the jet from the integrated intensity of the Q(v_1) Raman band at $\approx$3657 cm^{-1} by comparison with a reference static sample ($\approx$10 mbar) of H_2O (gas) in the expansion chamber. The $n(z)$ data measured at steps $\Delta z = 100\,\mu$m along the jet are shown in Figure 4. From the hydrodynamical point of view, the flow behaves as a nearly pure helium jet of $\gamma = 1.6577$ heat capacity ratio, as shown by the isentropic gas dynamic simulation in Figure 4. The excellent agreement between simulation and experiment excludes significant dissipative contributions to the flow (Montero 2013) and confirms the isentropic behavior of the jet. This enables obtaining the translational temperatures along the jet with fairly good accuracy from the measured number densities $n(z)$ by means of the isentropic relation

$$T_t(z) = T_0(n(z)/n_0)^{\gamma-1}, \tag{7}$$

where T_0 and n_0 are the stagnation conditions. Translational temperatures $T_t(z)$ are included in Figure 4. The estimated uncertainties for n are $\approx$3% at 120 K and $\approx$8% at 20 K. The corresponding uncertainties for T_t are $\approx$2 K and $\approx$1 K.

The populations of rotational levels, $P_i(z)$, were measured from the simulation of the complex rotational profile of the Q(v_1) Raman band of H_2O. Derivatives dP_i/dz were obtained from the $P_i(z)$ data by means of ad hoc exponential type fit

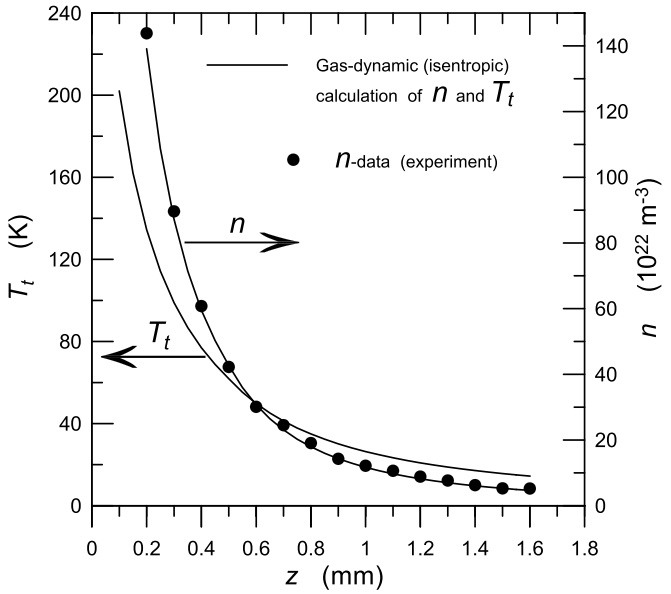

Figure 4. Experimental (•) and isentropic gas-dynamic simulation of number density n and translational temperature T_t along the He + H_2O(1.4%) supersonic jet for the nominal stagnation conditions $D = 350\,\mu$m, $p_0 = 309.7$ mbar, $T_0 = 360.3$ K, $\gamma = 1.6577$, and origin $z_0 = -49\,\mu$m.

functions. The local flow velocity $v(z)$ was determined from the energy-conservation relation (Tejeda et al. 2012)

$$v^2 = \frac{R}{\langle W\rangle}[5(T_0 - T_t) + 3\alpha(T_0 - \tilde{T}_r)], \tag{8}$$

where $R = 8.3145$ J K^{-1} mol^{-1} is the universal gas constant, and $\langle W\rangle = \alpha W(H_2O)+(1-\alpha)W(He)$ is the average molar mass of the mixture, with $\alpha = 0.014$ in our case; $\tilde{T}_r$ is an effective rotational temperature derived from the rotational populations P_i. The uncertainty of $v(z)$ is smaller than 1%. Flow velocities $v(z)$ enable expressing the rotational populations P_i in the time domain via the transformation $dP_i/dt = v\ dP_i/dz$. More details about instrumentation and measurement procedure can be found elsewhere (Fonfría et al. 2007; Pérez-Ríos et al. 2011; Tejeda et al. 2012).

The present work, which is based on a supersonic jet of 1.4% H_2O diluted in helium, poses, however, a number of specific difficulties which deserve further mention. To start, H_2O supersonic jets show a marked tendency toward condensation

(Tejeda et al. 2012; Li et al. 2014), with the result of a thermal increment in the jet which might bias its energy balance, invalidating the experimental rotational populations P_i in the MEQ (1). To avoid this undesired effect, the nozzle was operated at temperature $T_0 = 360.3$ K. The stagnation pressure and number density were $p_0 = 309.7$ mbar and $n_0 = 622.7 \times 10^{22}$ m^{-3}, sufficiently low to reduce condensation to undetectable limits (Tejeda et al. 2012; Li et al. 2014).

An additional difficulty found along the present work is the non-Boltzmann character of the rotational populations P_i along the supersonic jet, which becomes a more pronounced effect for lower translational temperatures and for higher rotational levels. This non-Boltzmann behavior can introduce numerical errors in the P_i's of the MEQ (1), and indirectly in the k's multiplying them. This implies that the determination of the actual populations P_i requires a fine analysis and numerical simulation of the complex profile of the Q(ν_1) Raman band of H_2O spanning from 3640 to 3658 cm^{-1}. For this purpose, we have employed a detailed tabulation of Raman cross sections (Avila et al. 2004). A sample of this simulation procedure at the point $z = 300\,\mu$m of the jet ($T_t = 100$ K) is shown in Figure 5. At this point, the accuracy of the populations P_i is on the order of ± 0.001, and the accuracy of the derivatives dP_i/dt, the LHT$_i$ of MEQ (1), is $\approx \pm 5000$ s^{-1}. As a whole, more than 1000 Raman spectra, each of 30–180 s, were recorded in order to generate the raw data needed in the present analysis.

Finally, since the Raman scattering cross section of H_2O is very small ($\approx 10^{-30}$ cm^{-2} sr^{-1}), the Raman signal in the jet is very weak, typically 1 to 10 photon s^{-1} for the weakest lines, which is not sufficient for recording good quality spectra at H_2O dilution below 1.4%. Therefore, the effect of H_2O:H_2O self-collisions, though marginal, must be considered. A second helium supersonic jet expanded through the same nozzle at $p_0 = 57.4$ mbar and $T_0 = 363.1$ K, enriched with 34% H_2O, has been employed for this purpose. Average effective rates derived from this jet for H_2O:H_2O self-collisions show that their contribution to the experimental LHT of the MEQ (1) of the highly diluted He + H_2O(1.4%) jet amounts to $6\% \pm 1.5\%$ at 20 K and $3\% \pm 1.5\%$ at 120 K. For convenience, we have taken an average value of $4.5\% \pm 3.0\%$ for the whole range 20–120 K, accumulating these additional uncertainties in the final rates. Consequently, the values of the experimental rates obtained according to Equation (5) have been multiplied by 0.955 in order to correct for the H_2O:H_2O self-collisions.

4. DISCUSSION

As inferred from Table 2, the χ^2 minima of the G-rates for ortho-H_2O:He and para-H_2O:He collisions are found in the ranges $1.41 \leqslant F_G^{\rm ortho} \leqslant 1.62$ and $1.12 \leqslant F_G^{\rm para} \leqslant 1.66$, respectively. The average values are $\tilde{F}_G^{\rm ortho} = 1.49 \pm 0.08$ and $\tilde{F}_G^{\rm para} = 1.30 \pm 0.20$, which reduce to $\tilde{F}_G^{\rm ortho} = 1.42 \pm 0.08$ and $\tilde{F}_G^{\rm para} = 1.24 \pm 0.19$ after correcting for the H_2O:H_2O self-collisions. These figures strongly suggest that in the $20 \leqslant T_t \leqslant 120$ K range the theoretical G-rates based on the G-PES are on average too small by $\approx (40 \pm 8)\%$ for ortho-H_2O:He, and $\approx (24 \pm 19)\%$ for para-H_2O:He collisions compared to experiment.

The H-rates and P-rates are closer to the experiment. After correcting for H_2O:H_2O self-collisions, we obtain from Table 2 $\tilde{F}_H^{\rm ortho} = 1.10 \pm 0.05$, $\tilde{F}_H^{\rm para} = 0.97 \pm 0.15$, $\tilde{F}_P^{\rm ortho} = 0.98 \pm 0.08$, and $\tilde{F}_P^{\rm para} = 0.92 \pm 0.09$. These figures show that both sets, H-rates and P-rates, agree with the experiment within $\approx 15\%$ in the $20 \leqslant T_t \leqslant 120$ K range. However, it is not possible to decide unambiguously from Table 2 whether the H-PES or the P-PES provides globally better rates. Far more detailed information can be derived from the supplementary tables, where the calculated G-rates, H-rates, and P-rates are tabulated jointly with their experiment-scaled counterparts. Table 3 is a guidance sample. They reveal a fundamental feature of the present methodology, namely, that the dispersion of the experiment-scaled rates is significantly smaller than the dispersion of the three original sets of calculated rates. Supplementary tables allow for detailed statistics (by energy levels or by temperatures, for instance) by comparing the calculated H-rates and P-rates with the experimental ones, $k_{\ell \to i}^{\rm SE}$, given in the last column. They are also useful for calculating excitation rates by means of Equation (3), or to compare rates calculated by other authors. For instance, the present P-rates calculated by us agree well with those by Yang et al. (2013), however, our set includes more elementary processes.

Finally, it should be noted from Table 2 that the statistical dispersion of the scaling factors F are in general larger for para-H_2O:He than for ortho-H_2O:He rates, consistently with the 1 to 3 para-H_2O to ortho-H_2O abundance in natural H_2O employed in the experiment. This is clearly reflected in Figure 5, where most Raman lines of para-H_2O transitions are overlapped by more intense lines of ortho-H_2O transitions.

5. RESULTS AND FINAL COMMENTS

An overview of the collisional problem of water with helium in the thermal range 20–120 K is reported in this work. We show that the combination of state-of-the-art Raman spectroscopy in supersonic jets with close-coupling calculations involving three different H_2O–He PESs provides a powerful methodology capable of establishing experimental STS rates of accuracy on the order of 10%.

The set of deexcitation rates for ortho-H_2O:He and para-H_2O:He collisions, scaled by the experiment and averaged according to Equation (5) (corrected for H_2O:H_2O self-collisions), is given online, a sample of which is given here in Table 4. The reported 1σ uncertainties for each individual collision process include all non-systematic experimental errors described in Section 3 through the scaling factors F_G, F_H, and F_P as well as other uncertainties derived from their respective PESs. A figure of merit of these results can be inferred from the average uncertainty of the dominant rates, here arbitrarily chosen as the 20 largest rates at a given temperature. The 1σ uncertainties for such rates in ortho-H_2O:He collisions are 5% at 120 K and 10% at 20 K. For para-H_2O:He the corresponding figures are 7.5% and 12%. Intermediate percentages are obtained for $20 < T_t < 120$ K.

As a representative sample, the theoretical and experimental STS rates for deexcitation processes starting and ending in the $i = 5$ rotational level of ortho-H_2O are shown in Figures 6 and 7, respectively. Note that the various STS rates involved in the population or depopulation of $i = 5$ rotational level range within two orders of magnitude, a feature which is well accounted for by the present methodology. Similar graphics for other rates can be generated from the online tables.

The present results are just a starting point to the H_2O:He collisional problem, where some room for accuracy improvement is still possible by new measurements in helium supersonic jets seeded with different concentrations of water. In any case, we hope that the tables reported here will prove useful for astrophysical applications, also serving as a guide for future theoretical works concerning the study of H_2O:He collisions.

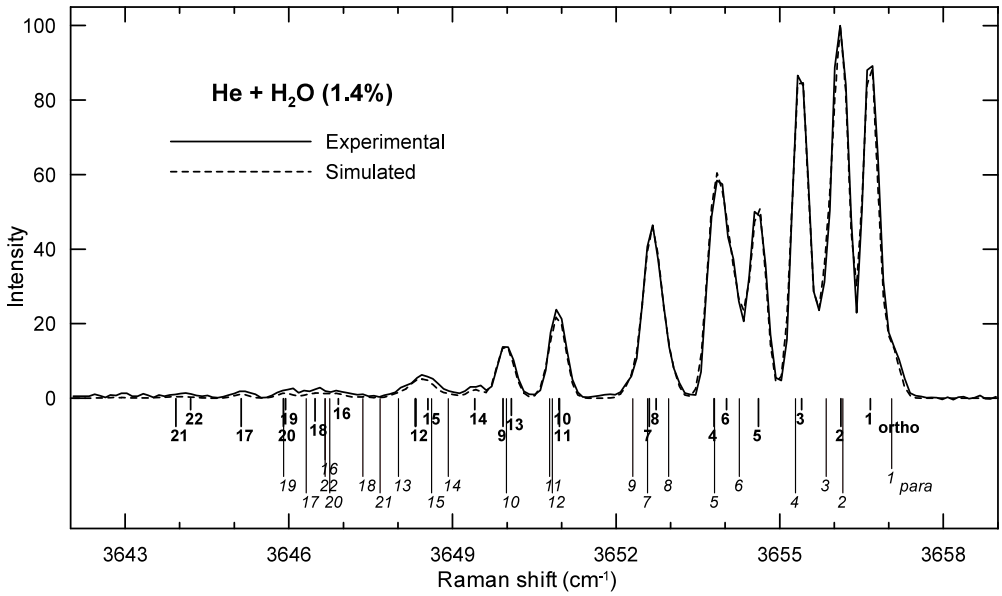

Figure 5. Experimental and simulated Raman spectra of H_2O, Q(ν_1)-branch, in the He + H_2O (1.4%) supersonic jet at point $z = 300\,\mu$m ($T_t = 100$ K). Intensity is in arbitrary units.

Table 3
Calculated and Experiment-scaled $k_{\ell\to i}$ Rates for Ortho-H_2O:He Collisions

					Calculated			Experiment-scaled			
$\ell \to i$	J_ℓ	J_i	$E_\ell - E_i$	T_t	G-rates	H-rates	P-rates	G-rates	H-rates	P-rates	$k^{\rm SE}_{\ell\to i}$-rates
2→1	1	1	18.6	20	641	740	1232	992	827	1153	991 ± 168
3→1	2	1	55.7	20	1070	1604	1821	1655	1792	1704	1717 ± 72
4→1	2	1	111.1	20	31	57	70	48	64	66	59 ± 10
5→1	3	1	113.0	20	139	141	154	215	158	144	172 ± 39
6→1	3	1	149.6	20	18	33	33	28	37	31	32 ± 5
7→1	3	1	188.4	20	29	58	64	45	65	60	57 ± 11
8→1	4	1	201.0	20	98	168	148	152	188	139	159 ± 26
9→1	3	1	261.6	20	1	1	0	2	1	0	1 ± 1
10→1	4	1	276.6	20	6	13	12	9	15	11	12 ± 3

Notes. $\ell = 2$ to 13; $\ell > i$; $i = 1$ to 8 for $T_t = 20, 40, 60, 80, 100, 120$ K. Homologous rates for para-H_2O:He collisions are provided in the machine-readable table.
Units: $E_\ell - E_i$ is in cm^{-1}, T_t in Kelvin, and rates in 10^{-14} cm^3 s^{-1}. 1σ uncertainties defined according to Equation (6) incremented by 3% due to the error from H_2O:H_2O self-collisions.

(This table is available in its entirety in a machine-readable form.)

Table 4
Experimental $k^{\rm SE}_{\ell\to i}$ Deexcitation Rates for Ortho-H_2O:He Collisions

$\ell \to i$	J_ℓ	J_i	$E_\ell - E_i$	20 K	40 K	60 K	80 K	100 K	120 K
2 → 1	1	1	18.6	991 ± 168	1302 ± 130	1918 ± 170	2279 ± 153	2894 ± 192	3512 ± 213
3 → 1	2	1	55.7	1717 ± 72	1738 ± 54	2171 ± 59	2322 ± 40	2743 ± 66	3162 ± 80
4 → 1	2	1	111.1	59 ± 10	76 ± 11	116 ± 14	144 ± 18	194 ± 24	248 ± 32
3 → 2	2	1	37.1	726 ± 180	701 ± 164	805 ± 174	798 ± 182	874 ± 194	944 ± 216
4 → 2	2	1	92.5	811 ± 61	927 ± 45	1246 ± 41	1403 ± 26	1716 ± 39	2033 ± 48
5 → 2	3	1	94.4	527 ± 47	532 ± 44	656 ± 39	690 ± 40	796 ± 38	898 ± 44
4 → 3	2	2	55.4	1001 ± 54	1050 ± 40	1332 ± 57	1434 ± 42	1694 ± 58	1948 ± 60
5 → 3	3	2	57.3	1283 ± 6	1298 ± 49	1623 ± 81	1733 ± 73	2048 ± 95	2362 ± 101
6 → 3	3	2	93.9	436 ± 34	466 ± 35	600 ± 34	659 ± 41	796 ± 40	936 ± 43

Notes. $\ell = 2$ to 13; $\ell > i$; $i = 1$ to 8 for $T_t = 20, 40, 60, 80, 100, 120$ K. Homologous rates for para-H_2O:He collisions are provided in the machine-readable table.
Units: $E_\ell - E_i$ is in cm^{-1}, and rates in 10^{-14} cm^3 s^{-1}. 1σ uncertainties defined according to Equation (6) incremented by 3% due to the error from H_2O:H_2O self-collisions.

(This table is available in its entirety in a machine-readable form.)

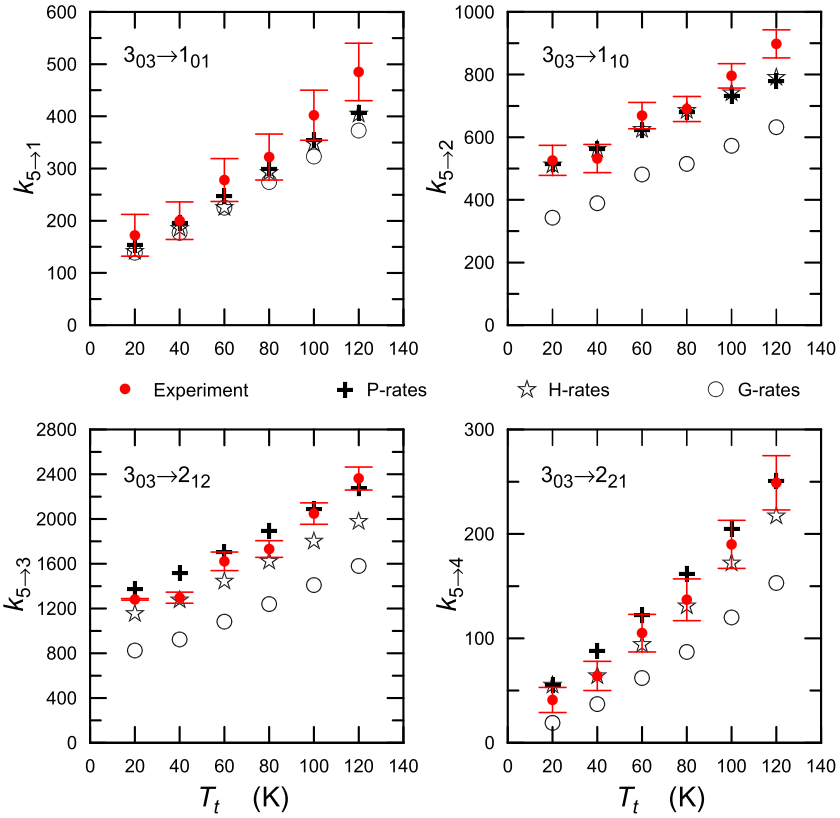

Figure 6. $k_{5\rightarrow i}$ deexcitation rates of ortho-H_2O:He inelastic collisions starting in the $i = 5$ rotational level of ortho-H_2O in units of 10^{-14} cm^3 s^{-1}.

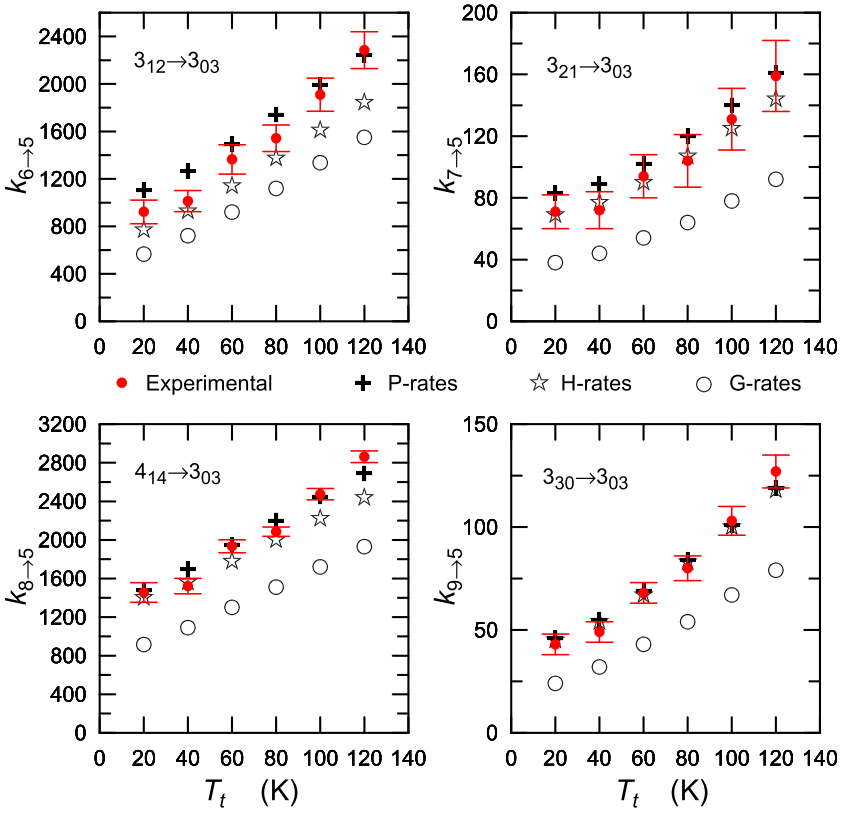

Figure 7. $k_{r\rightarrow5}$ deexcitation rates of ortho-H_2O:He inelastic collisions ending in the $i = 5$ rotational level of ortho-H_2O in units of 10^{-14} cm^3 s^{-1}.

This work has been supported by the Spanish Ministerios de Innovación (MICINN) and Economía y Competitividad (MINECO) through the research projects FIS2010-22064-C01, FIS2010-22064-C02, FIS2013-48275-C2-1-P, and FIS2013-48275-C2-2-P, and CONSOLIDER-ASTROMOL CSD2009-0038.

REFERENCES

Avila, G., Fernández, J. M., Tejeda, G., & Montero, S. 2004, JMoSp, 228, 38
Brudermann, J., Steinbach, C., Buck, U., Patkowski, K., & Moszinski, R. 2002, JChPh, 117, 11166
Calderoni, G., Cargnoni, F., & Raimondi, M. 2003, CPL, 370, 233
Dick, M. J., Drouin, B. J., & Pearson, J. C. 2009, JQSRT, 110, 619
Dick, M. J., Drouin, B. J., & Pearson, J. C. 2010, PhRvA, 81, 022706
Fonfría, J. P., Ramos, A., Thibault, F., et al. 2007, JChPh, 127, 134305
Green, S., Maluendes, S., & McLean, A. D. 1993, ApJS, 85, 181
Hodges, M. P., Wheatley, R. J., & Harvey, A. H. 2002, JChPh, 116, 1397
Hutson, J. M., & Green, S. 1994, MOLSCAT Computer Code, version 14, Distributed by Collaborative Computational Project No. 6 of the UK Science and Engineering Research Council (UK)
Li, Z., Borner, A., & Levin, D. A. 2014, JChPh, 140, 224501
Makarewicz, J. 2008, JChPh, 129, 184310
Maluendes, S., McLean, A. D., & Green, S. 1992, JChPh, 96, 8150
Montero, S. 2013, PhFl, 25, 056102
Palma, A., Green, S., DeFrees, D. J., & McLean, A. D. 1988, JChPh, 89, 1401
Patkowski, K., Korona, T., Moszinski, R., Jeziorski, B., & Szalewicz, K. 2002, JMoSt TEOCHEM, 591, 231
Pérez-Ríos, J., Tejeda, G., Fernández, J. M., Hernández, M. I., & Montero, S. 2011, JChPh, 134, 174307
Roncaratti, L. F., Belpassi, L., Cappelletti, D., Pirani, F., & Tarantelli, F. 2009, JPhChA, 113, 15223
Roueff, E., & Lique, F. 2013, Chem. Rev., 113, 8906
Tejeda, G., Fernández, J. M., & Montero, S. 2012, in AIP Conf. Proc. 1501, Proc. 28th Internat. Symp. Rarefied Gas Dynamics, Zaragoza (Spain), ed. M. Mareschal & A. Santos (Melville, NY: AIP), 1305
Tennyson, J., Zobov, N. F., Williamson, R., Polyanski, O. L., & Bernath, P. F. 2001, JPCRD, 30, 735
WISH: Water in Star-forming Regions with Herschel 2010, http://www.strw.leidenuniv.nl/WISH/
Yang, C. -H., Sarma, G., ter Meulen, J. J., et al. 2010a, JChPh, 133, 131103
Yang, C. -H., Sarma, G., ter Meulen, J. J., et al. 2010b, JPhChA, 114, 9886
Yang, B., Nagao, M., Satomi, W., Kimura, M., & Stancil, P. C. 2013, ApJ, 765, 77